NMR Studies of Low-Spin Ferric Complexes of Natural Porphyrin Derivatives. 4. Proton Relaxation Characterization of the Dimer Structure of Dicyanohemin in Aqueous Solution

Gerd N. La Mar,*[1] M. J. Minch, and J. S. Frye[1]

Contribution from the Departments of Chemistry, University of California, Davis, California 95616, and University of the Pacific, Stockton, California 95211.
Received December 22, 1980

Abstract: Concentration dependent chemical shifts, line widths, and spin-lattice relaxation rates of dicyanohemin at pH 9 can be attributed to intermolecular paramagnetic dipolar relaxation processes within a stereospecific dimer. The r^{-6} dependence of the relaxation rates permits determination of the dimer structure which consists of overlap of presumably parallel porphyrin planes (~5-Å separation) with the 2-vinyl and 3-methyl groups of each prophyrin in contact with the aromatic π-system of the other porphyrin and the propionate side sections extending into the solvent. This structure points to the important role of hydrophobic interactions in stabilizing the dimer. At higher pH values, particularly at higher temperatures (>25 °C), the dicyanohemin undergoes displacement of cyanide by one or more hydroxide ions.

The dimerization of metalloporphyrins in solution involves stacking of large polarizable porphyrin π-systems[2]. Dimer geometries vary widely with the nature of the metal ion, porphyrin substituents and axial ligands.[2-9] Three limiting types of porphyrin interactions are illustrated in Figure 1. A depicts complete overlap (4 on 4) of the porphyrins, B implies overlap of 2 pyrroles (2 on 2) on each porphyrin, and C features overlap of one pyrrole (1 on 1) of each porphyrin. Nuclear magnetic resonance spectroscopy has been used to elucidate the structures of metalloporphyrin dimers in solution, and examples of all three limiting types of interactions have been found. Concentration-dependent chemical shifts for diamagnetic porphyrin systems are consistent with face-to-face (A in Figure 1) or slightly slipped structures,[2-4] but ring currents alone do not lend themselves to analysis in quantitative terms. In the interesting and important class of iron porphyrin complexes, the presence of seven paramagnetic forms in the eight characterized oxidation/spin states has necessitated exploring other methods for obtaining structural information on the solution aggregates.

We have proposed recently[5] that the iron-proton dipolar relaxation, given in the fast motion limit by eq 1, where Q depends

$$R_1^{-1} = T_2^{-1} = Qr^{-6}T_{1e} \qquad (1)$$

only on the spin state, r is the iron-proton distance, and T_{1e} is the iron spin relaxation time, may provide a general method for effecting such solution structural analyses. While only a single, averaged resonance is observed per set of nonequivalent protons in the porphyrin monomer due to rapid exchange between monomer and dimer environment, the concentration-dependent relaxation rates can be separated into their intra- and intermolecular contributions whose ratios directly yield the intermolecular distance needed to describe the dimer geometry. We have demonstrated that this method can be used to determine quantitative dimer structures in solution and have emphasized that this method is particularly effective for elucidating highly stereospecific dimer interactions.[5-8] Intermolecular dipolar relaxation rates provided solution structural information on aggregates for both high-spin[8] and low-spin[5,6] ferric porphyrins as well as novel intermediate-spin ferrous complexes. Dimer geometries have varied from nearly four-on-four complete overlap[7] (A in Figure 1) to two-on-two overlap[7,8] (B) and the unusual one-on-one pyrrole[5,6] overlap depicted in C in Figure 1. In some cases, the same complex adopts different structures at different concentrations.[7]

The most flexible and interesting system has proven to be the low-spin dicyanohemin derivatives [1]. Analysis of concentration-dependent shifts has demonstrated the presence of only dimers[6] in methanol and methylene chloride, and the intermolecular relaxation was analyzed in terms of primarily one-on-one π-overlap involving the strongest π-donor (IV) and π-acceptor pyrroles (I).[5] Solvation effects were shown to be unimportant, and the dominance of electronic effects was emphasized by the ability to control the sterospecificity of the dimer interaction by changing the degree of in-plane asymmetry in the π electronic structure with different 2,4-substitutents.[6,9]

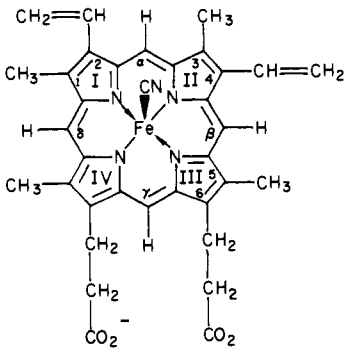

1

As part of our continuing efforts to expand the scope of paramagnetic dipolar relaxation as a solution structural tool and to explore the variety of factors which can control the geometry of a porphyrin dimer in solution, we have extended our proton NMR relaxation studies to the solution properties of the low-spin ferric dicyanoprotohemin complex (1) in aqueous medium. In contrast to previously studied solvents,[5] we anticipated that hydrophobic rather than electronic factors may play a focal role in determining the structure of the solution aggregate. The relative

(1) University of California.
(2) White, W. I. In "The Porpyrins"; Dolphin, D., Ed.; Academic Press: New York 1978; Vol. V, Part C, pp 303-339.
(3) Abraham, R. J.; Evans, B.; Smith, K. M. *Tetrahedron* **1980**, *34*, 1213.
(4) Abraham, R. J.; Fell, S. C. M.; Pearson, H.; Smith, K. M. *Tetrahedron* **1979**, *35*, 1759 and references therein.
(5) Viscio, D. B.; La Mar, G. N. *J. Am. Chem. Soc.* **1978**, *100*, 8092.
(6) Viscio, D. B.; La Mar, G. N. *J. Am. Chem. Soc.* **1978**, *100*, 8096.
(7) Migita, K.; La Mar, G. N. *J. Phys. Chem.* **1980**, *84*, 2953.
(8) Synder, R. V.; La Mar, G. N. *J. Am. Chem. Soc.* **1977**, *99*, 7178.
(9) La Mar, G. N.; Viscio, D. B.; Smith, K. M.; Caughey, W. S.; Smith, M. L. *J. Am. Chem. Soc.* **1978**, *100*, 8085.

0002-7863/81/1503-5383$01.25/0

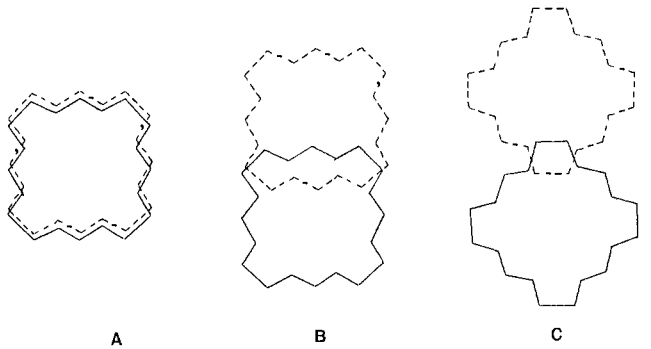

Figure 1. Various types of ring overlap in porphyrin dimers: A, four-on-four; B, two-on-two, and C, one-on-one pyrrole overlap.

propensity for hydrophobic vs. hydrophilic interaction of various portions of the iron protoporphyrin IX prosthetic group are critical for proper orientation of the prosthetic group in the heme pocket of b-type hemoproteins.[10]

Experimental Section

Purchased samples of hemin chloride (Porphyrin Products) were shown by NMR to be free from impurities and were used without additional purification. Solutions of the cyanide complex were prepared by dissolving hemin in 0.05 M KCN with 0.05 M NaO^2H in ^2H_2O (>99%). The phenomenological pH was adjusted by dropwise addition of 0.1 M ^2HCl. The pH was measured at 25 °C in the NMR tube with an Ingold microcombination electrode and a pH meter before and after each run. The reproducibility of pH measurement was ±0.02 unit. The pH values were not corrected for the isotope effect.

Optical spectra were determined on a Cary 17 recording UV-vis spectrophotometer with quartz cuvetts and a thermostated cell compartment.

^1H NMR spectra were obtained on a Nicolet 360-MHz pulsed FT NMR spectrometer using up to 32K points over a 20-KHz bandwidth. ^{13}C NMR spectra were obtained on a Nicolet 200-MHz spectrometer operating at 50.3 MHz. Chemical shifts were measured vs. the residual water line which was calibrated as a function of temperature and pH to DSS, 4,4-dimethyl-4-silapentanesulfonate. Line widths were taken as widths at half-intensity determined by least-squares Lorentzian line fits to base line straightened spectra. Spin-lattice relaxation rates, $R_1 = T^{-1}$, were measured by using a 180°-τ-90° inversion recovery technique where τ is the time interval between the 180° and 90° pulses. The delay between successive accumulations was at least $10T_1$ and the phase of the 90° pulse was alternated to minimize systematic errors due to inaccuracies in pulse length, RF field inhomogeneity, and off-resonance effects.[11] Linear ($\rho > 0.99$) semilogarithmic plots of ln $(I_\infty - I_\tau)$ against τ with slopes $-R_1$ were obtained. The uncertainties in R_1, given in Table II, are based on the reproducibility of duplicate measurements.

The dilution shifts were analyzed for dimer formation ($2M \rightleftharpoons D$) by iterative computer fit to eq 2, where $(\Delta\nu/\nu)_{obsd}$, $(\Delta\nu/\nu)_D$, and $(\Delta\nu/\nu)_M$

$$\left(\frac{\Delta\nu}{\nu}\right)_{obsd} = \left(\frac{\Delta\nu}{\nu}\right)_M + \left[\left(\frac{\Delta\nu}{\nu}\right)_D - \left(\frac{\Delta\nu}{\nu}\right)_M\right]\frac{(4KC + 1 - \sqrt{8KC + 1})}{4KC} \quad (2)$$

are the observed chemical shift and that for the pure dimer and monomer, respectively, C is the total hemin concentration, and $K = [D]/[M]^2$.

Results and Discussion

The chemical shifts and line widths of **1** depend on pH, temperature, and concentration of **1**. We found it necessary to characterize the equilibria between the dicyano species (**1**) and other species resulting from the displacement of cyanide by one or more hydroxide ions, in order to assure that the dimerization reaction can be studied without interference from species other than **1**. At pH 9 at 25 °C or lower, the chemical shift and line width changes as a function of hemin concentration can be explained entirely in terms of dimerization of **1**. At higher pH values the NMR spectra indicate the onset of a rapid equilibration between **1** and some mixed-ligand species, possibly structure, **2** as well as slow exchange with the previously characterized[12,13] dihydroxy dimer **3**.

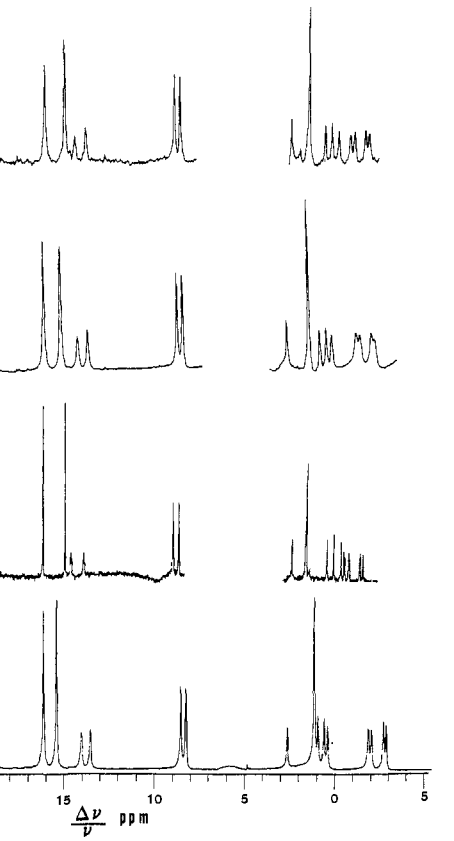

Figure 2. The 360-MHz traces of A (0.01 M hemin (pH 9)), B (0.0002 M hemin (pH 9)), C (0.01 M hemin (pH 11.6)), and D (0.01 M hemin (pH 11.8)). All in ^2H_2O with 0.05 M KCN and 0.05 M NaO^2H-NaCl at 25 °C.

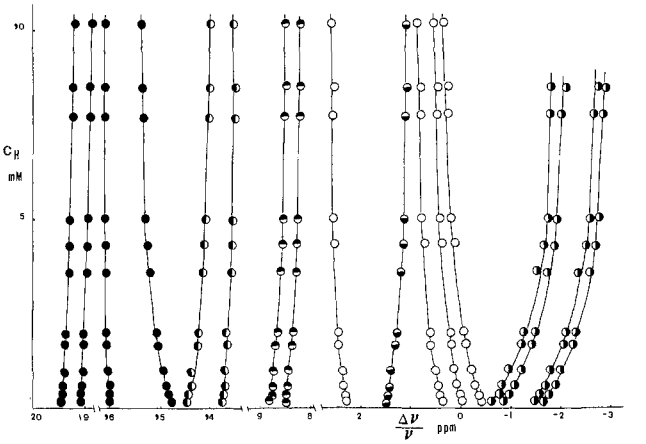

Figure 3. The concentration dependence of the chemical shifts of hemin $(CN)_2$ in ^2H_2O with 0.05 M KCN and 0.05 M NaO^2H-NaCl (pH 9) at 25 °C: ●, H methyls; ◐ α-vinyls; ⊖, α-CH_2; ○ meso protons; ⊖, β-CH_2; ◑, β-vinyl protons.

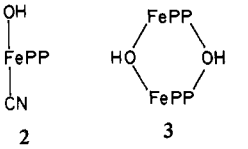

2 3

(10) Antonini, E.; Brunori, M. In "Hemoglobin and Myoglobin and Their Interaction with Ligands", North-Holland Publishing Co.: Amsterdam, 1971; Chapter 4.

(11) Martin, M. L.; Martin, G. J.; Delpuech, J. J. "Practical NMR Spectroscopy"; Heyden Press: London, 1980; p 257.

(12) Goff, H.; Morgan, L. O. *Inorg. Chem.* **1976**, *15*, 2062.

(13) Blauer, G.; Ehrenberg, E. *Biochim. Biophys. Acta* **1966**, *112*, 496.

Table I. Concentration Dependence of Hemin$(CN)_2$ ^1H Chemical Shifts[a]

resonance[b]	0.0002 M hemin	0.01 M hemin
8-Me	19.49	19.18
5-Me	19.10	18.83
3-Me	16.10	16.06
1-Me	14.77	15.33
2-α-vinyl	14.46	13.96
4-α-vinyl	13.76	13.50
α-CH_2	8.81, 8.48	8.47, 8.18
γ-meso	2.28	2.55
β,δ-meso	0.35, −0.03	0.84, 0.51
α-meso	−0.44	0.31
β-CH_2	1.49	1.05
2-β-vinyl	−0.61, −0.87	−1.89, −2.12
4-β-vinyl	−1.48, −1.66	−2.77, −2.90

[a] Shifts in ppm (±0.003 ppm) referenced to DSS, at 25 °C for hemin in ^2H_2O, 0.05 M KCN with 0.05 M NaO^2H–NaCl (pH 9). [b] See ref 5 for resonance assignments.

The concentration-dependent chemical shift and line width changes upon dimerization are illustrated in Figure 2 which gives the 360-MHz ^1H NMR trace of 0.01 M **1**, A (mostly dimer) and 0.0002 M **1**, B (mostly monomer), both with 0.05 M KCN and 0.05 M NaO^2H–NaCl in ^2H_2O (pH 9.0) at 25 °C. The chemical shifts are plotted as a function of hemin concentration in Figure 3, and the net changes in the NMR of **1** observed for a 50-fold increase in the concentration of **1** at pH 9 (25 °C) are given in Table I. Although the various resonances shift by different amounts and in different directions at pH 9, all changes occur over the same concentration range and the linewidth increases for the methyl and mesoprotons have the same concentration dependence as the chemical shifts. The large changes observed for the meso-H_α, both meso-H_β, $-H_\delta$, and the four vinyl-H_β resonances can be fitted to eq 2 by iterative computer methods to yield K, the equilibrium constant for dimer formation. The calculated equilibrium constant was 2×10^2 L/mol (25 °C) regardless of the resonance monitored.

Ligand-Exchange Reactions. At higher pH values the linewidths for all resonances of 0.01 M hemin$(CN)_2$ broaden, decrease in intensity and shift. New peaks corresponding to a high-spin dihydroxy dimer **3** appear downfield. In Figure 2 are the 360-MHz ^1H traces of 0.01 M hemin with 0.05 M KCN at pH 11.6 (C in Figure 2) and 11.8 (D in Figure 2). The chemical shift and line width of the methyl protons of **1** are given as a function of pH in Figure 4.

Species **1** and **3** differ in color and the equilibrium constant for their interconversion can be measured from the change in the optical spectrum of 1.18×10^{-4} M hemin in 0.10 M KOH with added KCN. The green species (λ_{max} = 385, 610 nm) observed in the absence of KCN is converted to the red dicyano complex (λ_{max} 423, 545 nm) with added KCN. There is an isobestic absorption wavelength at 590 nm, indicating that at these concentrations, no appreciable amount of a third species is present. The change in the optical spectrum as a function of KCN concentration is given in Figure 5. The change in absorbance at 545 nm can be related to the equilibrium constant[14] for the equilibrium

$$4CN^- + \underset{\mathbf{3}}{(\text{hemin})_2(OH)_2} \rightleftharpoons \underset{\mathbf{1}}{2\text{hemin}(CN)_2} + 2OH^-$$

with a K_F value for the formation of **1** from **3** of 0.34 ± 0.03 L/mol at 25 °C. Higher temperatures favor the green species and the equilibrium constants measured at five temperatures between 27.5 and 54 °C yield a nicely linear van't Hoff plot (correlation coefficient 0.998) with the parameters $\Delta H°$ = −20.1 kcal/mol, $\Delta S°$ = 66 eu, and $\Delta G°$ = 0.64 kcal/mol (25 °C). The large positive entropy implies a gain in translational freedom as the covalent dimer is dissociated. Hambright[15] has reported spectrophotometric titrations of cyanide with monomeric iron(III) hydroxy complexes of natural porphyrins in 2% sodium dodecylsulfate with similar spectroscopic changes.[16]

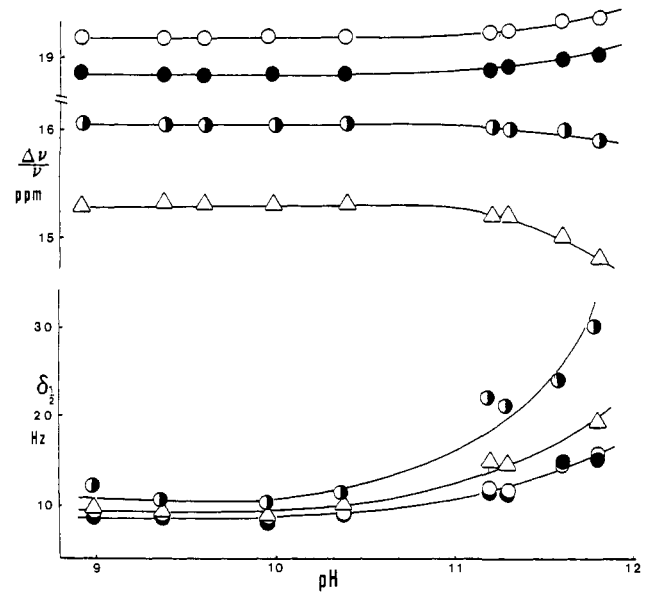

Figure 4. The pH dependence of the chemical shifts (A) and line widths (B) of 0.01 M hemin in ^2H_2O with 0.05 M KCN and 0.05 M NaO^2H–NaCl at 25 °C: ○, 8-methyls; ●, 5-methyls; ◑, 3-methyls; △, 1-methyl.

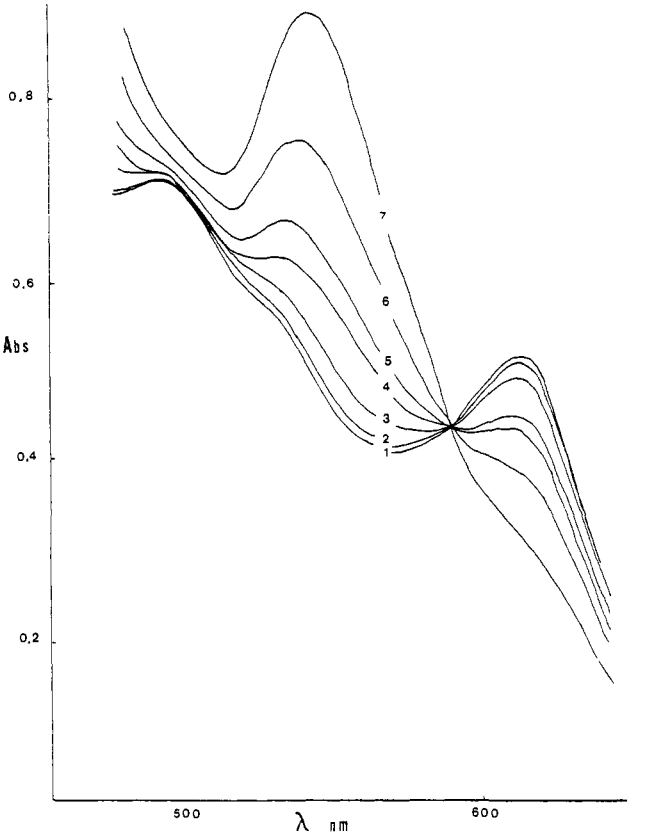

Figure 5. The optical spectrum of 0.118 mM hemin in 102 mM KOH in H_2O with various amounts of KCN. Curves 1 through 7 correspond to 0, 4.8, 12.0, 20.5, 26.2, 35.1, 47.7 mM KCN, respectively, at 25 °C.

(14) The concentration of **1** is related to the absorption at 545 nm by the expression $A_{obsd} = \epsilon_1[\mathbf{1}] + \epsilon_3([\mathbf{1}]_0 - [\mathbf{1}])/2$ where $[\mathbf{1}]_0$ represents the stoichiometric hemin concentration and ϵ_1 and ϵ_3 are the extinction coefficients for absorption at 545 nm determined in the presence of a large excess (>0.2 M) and in the absence of KCN respectively ($\epsilon_1 = 9.98 \times 10^3$ and $\epsilon_3 = 7.22 \times 10^3$ L/(M cm)). At KCN concentrations where both **1** and **3** are present, the equilibrium constant K_F for the formation of **1** from **3** is related to $[\mathbf{1}]_0$ and $[\mathbf{1}]$ by $K_F = [\mathbf{1}]^2[OH]^2/([CN]^4([\mathbf{1}]_0 - [\mathbf{1}])/2)$.

(15) Hambright, P.; Chock, P. B. *J. Inorg. Nucl. Chem.* **1975**, *37*, 2363.

Table II. Proton Spin-Lattice Relaxation Rates for Hemin(CN)$_2$

resonance	R_1^{obsd},[a] s^{-1}	R_1^{D},[b] s^{-1}	R_1^{inter}, s^{-1}	R_1^{inter}/R_1^{intra}	$r(H_a\text{-}Fe_b)$,[c] Å
1-CH_3	11.2 ± 0.2	11.7 ± 0.3	1.4 ± 0.5	0.14 ± 0.04	8.5 ± 0.4
3-CH_3	13.0 ± 0.2	13.8 ± 0.3	3.5 ± 0.4	0.34 ± 0.05	7.3 ± 0.2
5-CH_3	10.0 ± 0.2	10.3 ± 0.3	~0	~0	
8-CH_3	10.0 ± 0.2	10.3 ± 0.3	~0	~0	
meso-H_α	23.8 ± 0.5	25 ± 0.8	8.3 ± 1.9	0.51 ± 0.15	5.2 ± 0.4
meso-H_β, H_δ	19 ± 3	19.4 ± 3.2	*d*	*d*	*d*
meso-H_γ	16.7 ± 0.8	16.7 ± 1.1	~0	~0	

[a] $R_1 = T_1^{-1}$ (s^{-1}) for 0.0106 M hemin with 0.05 M KCN, 0.05 M NaO^2H-NaCl (pH 9) at 10 °C in ^2H_2O. [b] See ref 19. [c] Intermolecular proton-iron distance. [d] Large uncertainties in *meso*-H_β, H_δ relaxation rates precludes calculation of R_1^{inter}.

The optical and NMR studies both show that the concentration of **3** is negligible for pH values less than 10 at 25 °C or lower. The concentrations of **1** calculated from the equilibrium expression and those measured by integration of the 8-methyl peak of **1** fall on the same smooth curve with pH. The integration, line widths, and chemical shifts of the methyl protons of **1** are pH independent from 9 to 10 at 25 °C or lower. At higher temperatures, **3** is detectable at lower pH values; for example, the far downfield resonances due to **3** are apparent in the NMR spectrum of 0.01 M Hemin with 0.05 M KCN (pH 9.3) at 60 °C.

We see both species **1** and **3** in ^1H NMR spectra above pH 11, implying a slow exchange between them.[17] The line broadening and change in chemical shift observed for **1** above pH 10 at 25 °C or higher is not due to rapid exchange between **1** and **3** but point to rapid exchange between **1** and an intermediate such as **2**,[18] which is itself in slow exchange with **3**.

Chemical shift and line width effects due to the presence of **2** or **3** are unimportant at pH 9 if the temperature is 25 °C or lower. Under these conditions the chemical shift and line width as a function of hemin concentration can be explained entirely in terms of dimerization of **1**.

Dimer Structure. Qualitative Aspects. The chemical shift changes of all the resonances at pH 9 (25 °C) depend on hemin concentration in the same manner and yield the same equilibrium constant for dimer formation.[19] Moreover, the line width increases for the methyl and meso protons exhibit the same hemin concentration dependence as the chemical shift changes. This implies either a unique dimer structure or a number of dimer structures with equivalent stabilities (same K values) capable of similarly regioselective relaxation. The chemical shifts, although providing a more quantitative index of the thermodynamics of aggregation, are of very limited use in the structure determination of the dimer because downfield dipolar shifts and upfield ring current shifts can cancel above and below the porphyrin plane, precluding a quantitative analysis.[5-8] The relaxation rates, either line width ($\pi\delta = T_2^{-1}$) or T_1^{-1}'s, however, due to their r^{-6} dependence, can yield information on the dimer structure.

The paramagnetic line widths, $\delta \propto r^{-6}$, yield a qualitative picture of the dimer which contrasts sharply with the results previously obtained for the same complex in either methanol or methylene chloride.[5,6] Upon dimerization, the equally broad heme methyl peaks of the monomer broaden in the relative order

$$\delta(3\text{-}CH_3) > \delta(1\text{-}CH_3) > \delta(5\text{-}CH_3) \approx \delta(8\text{-}CH_3)$$

while the *meso*-H line widths increase in the order

$$\delta(H_\alpha) > \delta(H_\beta) \approx \delta(H_\delta) \gtrsim \delta(H_\gamma)$$

suggesting a pseudosymmetry about the α-γ meso axis in the dimer. Structure A in Figure 1 is easily elminated since it predicts equal intermolecular line broadening for each of the four methyls and the four meso-H's. The structure C, found exclusively for **1** in methanol and methylene chloride,[5,6] is eliminated since it requires comparable broadening for two heme methyls and pairwise broadening of two adjacent meso-H positions. The trends in intermolecular broadening for methyls and meso-H's, however, can be qualitatively rationalized by a structure such as B in Figure 1, where the vinyl bearing pyrroles are mutually overalapping and the propionic acid groups extend out into solution.

An additional difference between the intermolecular line broadening detected for **1** in ^2H_2O and in other solvents[5,6] is that in the present case, dimerization affects all line widths, suggesting that T_{1e} within eq 1 within a ferric porphyrin complex is altered upon incorporation into the dimer (vide infra).

Quantitative Aspects. Spin-lattice relaxation rates ($R_1 = T_1^{-1}$) parallel the resonance line widths and allow a quantitative refinement[5,6] of the dimer structure suggested by line widths. Table II gives the observed relaxation rates (R_1^{obsd}) of methyl and meso protons of 0.0106 M hemin in ^2H_2O with 0.05 M KCN (pH 9) at 10 °C. Also included in Table II are the corresponding relaxation rates calculated for the pure dimer (R_1^D).[21] The observed relaxation rates for all the methyl protons of 0.000 66 M hemin are 8.2 ± 0.5 s^{-1} and for the meso protons 17 ± 1 s^{-1}, which can be taken as an estimate of the relaxation rates for the pure monomer (R_1^M).

Evaluation of the observed concentration-dependent spin-lattice relaxation rates in terms of the dimer structure requires the assumption that the intrinsic relaxation within a porphyrin is more effective in a dimer than a monomer (vide infra). In fact, this is clearly demonstrated in that the dimer structure dictated by line widths places the 5-CH_3 and 8-CH_3, as well as meso-H_γ, for

(16) Hambright[15] reports a green monomeric iron(III) hydroxy protoporphyrin IX complex in equilibrium with the red dicyano complex. With SDS the equilibrium favors the dicyano complex much more than in our nonmicellar case.

(17) The chemical shift difference between the methyls of **1** and **3** is quite large (~30 ppm) so that the interconversion between **1** and **3** can be quite rapid but still within the NMR slow exchange limit. The predicted upper limit for an interconversion rate within the slow exchange limit is 6×10^4 s^{-1}. (The reported rate for the dissociation of aquated iron(III) dimers is about 10^3 s^{-1}, cf. Fleischer, E. B.; Palmer, J. M.; Srivastava, T. S.; Chatterjee, A. *J. Am. Chem. Soc.* **1971**, *93*, 3162.)

(18) Rapid exchange with an intermediate such as **2** contributes to the line widths and chemical shifts of the NMR resonances of **1** above pH 10 or at temperatures greater than 25 °C: i.e., the chemical shifts of the 8- and 5-methyls are shifted downfield while the 3- and 1-methyl resonances are shifted upfield with increasing pH (see Figure 5) and the methyl line widths do not broaden equally.

(19) Other dicyanoheme derivatives were also investigated briefly but failed to provide useful quantitative data. Dicyanodeuterohemin (2,4-proton substituents in **1**) also exhibited concentration-dependent shifts; however the shift changes were considerably smaller than for **1**, and limiting values were not attainable up to 0.01 M, precluding unambiguous determination of the degree of aggregation and its equilibrium constant. Moreover, dicyanodeuterohemin exhibited considerably reduced concentration-dependent line width. A much larger degree of aggregation of protohemin relative to deuterohemin or mesohemin (2,4-ethyl **1**) has been noted previously.[20] Since dicyanodeuterohemin also exhibited large 2,4-H shift change with concentration it may be assumed that the presumed dimer structure is similar to that determined here for **1**. Hence, hydrophobic forces are also important for deuterohemin but apparently to a much reduced degree compared to protohemin. The individual methyls of dicyanomesohemin have not been assigned, while dicyanodiacetyldeuterohemin is not stable at pH 9, and hence neither could be characterized for comparison in the manner previously done for these complexes in methanol.

(20) Brown, S. B.; Hatzikonstantinov, H. *Biochim. Biophys. Acta* **1979**, *585*, 143.

(21) The relaxation rates for the pure dimer (R_1^D) can be obtained by the expression $R_1^D = [R_1^{obsd} - (1 - \chi_D)R_1^M]/\chi_D$, where R_1^{obsd} and R_1^M are the observed spin-lattice relaxation rates at 0.0106 M and 0.000 66 M hemin in 0.05 M KCN, 0.05 M NaO^2H-NaCl (pH 9, 10 °C), where the dimer and monomer predominate, respectively. The mole fraction protons in the dimer χ_D was estimated to be 0.85 from plots of chemical shift vs. hemin concentration at 10 °C.

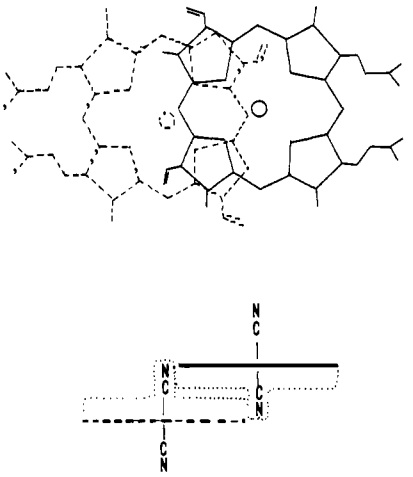

Figure 6. The geometry of the hemin$(CN)_2$ dimer corresponding to the interporphyrin distances in Table II. The distances determined are consistent with a geometry with pairwise interaction of pyrrole I and II of the first porphyrin with pyrroles II and I of the second.

one porphyrin so far from the iron of the second porphyrin that the increase in line widths and T_1^{-1}'s for these protons cannot arise from intramolecular relaxation and hence must arise from an increase in T_{1e} in eq 1. The relaxation rates of these remote groups provide an index of the intramolecular relaxation rate in the dimer.

The total dipolar spin–lattice relaxation rate for proton a in a dimer is the sum of *intramolecular* and *intermolecular* contributions

$$R_1^D(a) = R_1(a)^{intra} + R_1(a)^{inter} \quad (3)$$

Setting $R_1^D(5,8\text{-}CH_3) \equiv R_1$ (methyls)^{intra}, where $R_1^D(5,8\text{-}CH_3)$ is the relaxation rate of these protons in the dimer (second column in Table II), calculated from the observed relaxation rate,[21] and similarly setting $R_1^D(\text{meso-}H_\gamma) \equiv R_1(\text{meso-H})^{intra}$, we obtain, using eq 3, the $R_1(H)^{inter}$ for 1- and 3-CH_3 and meso-H_α, as listed in the third column of Table II. The observed relaxation rates for meso-H_β and meso-H_δ could not be obtained sufficiently accurately because of overlap with the hemin β-CH_2 resonance to warrant separation into *inter-* and *intramolecular* components. The ratio

$$R_1(a)^{inter}/R_1(a)^{intra} = r^6(H_a\text{–}Fe_a)/r^6(H_a\text{–}Fe_b), \quad (4)$$

(fourth column in Table II), together with the known[22] $r(H_a - Fe_a)$ for the heme methyl (6.1 Å) and a meso-H (4.6 Å), yield the last column of Table II.

The three spheres of radii 7.3, 8.5, and 5.2 Å centered at 3-CH_3, 1-CH_3, and meso-H_α for one porphyrin interesect within the specified uncertainties, ±0.3 Å, to define a region locating the iron of the second porphyrin in the dimer. Parallel porphyrin stacking consistent with these distances features an interplanar spacing of 4.8 ± 0.5 Å and an interiron separation of ~8 Å, as depicted in Figure 6. The structure resembles a two-on-two interaction with considerable slip along the α-γ-meso axis and is thus related more to that found for completely unligated ferrous porphyrin at higher concentration[7] than the same complex in more hydrophobic solvents.[5,6]

The dimer structure in Figure 6 also provides a basis for rationalizing the increase in T_{1e} in eq 1 for the dimer. Studies of the proton NMR spectra of monomeric **1** in different solvents have shown that both shifts and line widths depend on a specific interaction between the solvent and the coordinated cyanide.[23] Thus strong hydrogen-bonding donors such as water yielded the narrowest lines and smallest magnetic anisotropy, with both the line width and anisotropy increasing for more hydrophobic solvents.[23] The two internal cyanide ligands in the dimer are directed toward a point between the meso-H_α and the 2-vinyl-Hα, an environment hydrophobic compared to that experienced in the monomer (see Figure 6). Goff[24] has shown that the ^{13}C hyperfine shift for the coordinated cyanide also reflects the hydrophobicity of the solvent, with the peak moving upfield ~100 ppm on going from water to methanol.[24] In the present case, the bound ^{13}CN shift is located 2330-ppm upfield of $(CH_3)_4Si$ at 1.1 mM **1** (mostly monomer), which moves further upfield to 2366 ppm at 11 mM (mostly dimer), clearly indicating that the averaged bound cyanide environment is shifted into a more hydrophobic environment in the dimer. The chemical shift change is too large to result from ring current effects alone and the ^{13}CN line width is independent of hemin concentration ruling out intermolecular paramagnetic contributions due to the second iron. The small increases in 5,8-CH_3 and meso-H_γ line widths upon dimer formation are completely consistent with line width changes previously noted on taking monomeric **1** from H_2O to a less hydrophilic solvent.

The substantial difference in the structure of the dimer of **1** in water and other solvents such as methanol or methylene chloride[5,6] must be attributed to the hydrophobic nature of the porphyrin π-system. In both methanol and methylene chloride the presumed solvation of the π-system by the hydrophobic portion of the solvent permitted the nature of the interporphyrin interactions in the dimer to be dominated by electronic effects, i.e., interaction between the strongest π-acceptor and π-donor pyrroles.[5,6] The observation[5] that the same dimer structure obtains in methanol for either the free acid or diester emphasizes the unimportant role played by the hydrophilic propionate groups in this solvent. In aqueous solution the dimer structure appears to be governed primarily by hydrophobic interactions, where the interaction of the porphyrin π-cloud, particularly near the hydrophobic vinyl groups, and water is minimized by mutual pairwise overlap of pyrroles I and II. This structure permits maximum hydration of, and minimum electrostatic respulsion between, the two sets of propionates.[25]

Effect of Additives. The effects of added electrolyte (NaCl) which enhances dimerizations[26] and added $[^2H_4]$methanol which inhibits dimerizations at 25 °C are consistent with a dominant role for hydrophobic interactions in the dimer. For ionic strengths less than 0.15 M, the ^1H NMR changes can be entirely accounted for by a monomer–dimer equilibrium; additional electrolyte gives viscous solutions with broad lines suggesting higher aggregates. Added $[^2H_4]$methanol disrupts the dimer; as little as 25 mol % ^2H completely eliminates the line broadening due to dimerization and the chemical shifts change in the manner expected for monomeric **1** in a less polar solvent.[9]

Conclusion

The concentration-dependent line widths and spin–lattice relaxation rates of dicyanohemin in ^2H_2O can be interpreted in terms of highly regioselective intermolecular paramagnetic dipolar relaxation processes. The r^{-6} dependence of the relaxation rates permits the determination of the dimer structure which consists of the sterospecific overlap of pyrroles I and II of one porphyrin with pyrroles II and I of the other. The close spacing of presumed parallel porphyrin planes (~5 Å) and the contact of the 2-vinyl and 3-methyl groups of each porphyrin with the π-system of the other is consistent with hydrophobic interaction involving dispersion (i.e., van der Waals) forces between the aromatic π-system and the protons of the ring substituents. Dispersion forces involving aromatic π-systems have been shown to predominante in other hydrophobic interactions.[27]

(22) Scheidt, W. R., Haller, K.; Hatano, K. *J. Am. Chem. Soc.* **1980**, *102*, 3017.

(23) La Mar, G. N.; Del Gaudio, J.; Frye, J. S. *Biochim. Biophys. Acta* **1977**, *498*, 422.

(24) Goff, H. *J. Am. Chem. Soc.* **1977**, *99*, 7723.

(25) Although it has been asserted that protoferriheme dimer in water is stabilized by increased conjugation of the vinyl groups with the porphyrin ring in the dimer,[20] changes in the chemical shift of the α- and β-vinyl peaks do not indicate enhanced vinyl group–porphyrin coplanarity.[26] The observed change is consistent with a small upfield ring current contribution to the chemical shifts of the α- and β-vinyl protons possibly accompanied with greater out-of-plane orientation of the vinyls in the dimer.

(26) La Mar, G. N.; Viscio, D. B.; Gersonde, K.; Sick, H. *Biochemistry* **1978**, *17*, 361.

The importance of the hydrophobic interactions of pyrroles I and II and aliphatic and/or aromatic amino acid side chains in myoglobins and hemoglobins is evidenced by the evolutionary conservatism of these amino acids.[10] Although heterogeneity in hemin orientation within the pocket of hemoproteins is now recognized in several cases[28-30] all cases involve permutating pairwise the two hydrophobic (I ↔ II) and the hydrophilic pyrroles (III ↔ IV). The difference in hydrophobicity of the perimeter of pyrroles I, II and III, IV makes it extremely unlikely that heme rotational heterogeneity about the β-γ-meso axis will occur in a protein environment.

Acknowledgment. This work was supported by the National Science Foundation (Grant CHE-77-26517) and the UCD NMR Facility. M.J.M. gratefully acknolwedges the encouragement, resources, and support made available to him during his sabbatical leave, 1979-1980.

(27) Minch, M. J.; Sevenair, J. P. Henling, C. *J. Org. Chem.* **1979**, *44*, 3247.
(28) La Mar, G. N.; Budd, D. L.; Viscio, D. B.; Smith, K. M.; Langry, K. C. *Proc. Natl. Acad. Sci. U.S.A.* **1978**, *75*, 5755.
(29) La Mar, G. N.; Smith, K. M.; Gersonde, K.; Sick, H.; Overkamp, M. *J. Biol. Chem.* **1980**, *255*, 66.
(30) La Mar, G. N.; de Ropp, J. S.; Smith, K. M.; Langry, K. C. *J. Am. Chem. Soc.* **1980**, *102*, 4833.

Substituent Dependence of the Selectivity in Alkene Bromination through Bromocarbenium Ions[1]

Elisabeth Bienvenue-Goetz and Jacques-Emile Dubois*

Contribution from the Institut de Topologie et de Dynamique des Systèmes de l'Université Paris VII, associé au C.N.R.S., 75005 Paris, France. *Received December 1, 1980*

Abstract: Substituent effects on the rates of bromination of alkenes $G_\alpha R_\alpha C{=}CR_\beta R_\beta'$, where G is a conjugatively electron-donating group, are consistent with a carbenium ion like transition state, whereas by the same criteria the transition state for nonconjugated alkenes is bromonium type. The reactivities of compounds with the same substituent G are analyzed in terms of the sensitivity to structural and solvent effects. The lowest sensitivity is attributed to the earliest transition state. The dependence of the reaction constant on G leads to a general equation including cross terms: $\log k = -7.7\sum(\sigma_p^+)_\alpha - 13.7\sum(\sigma_m^+)_\beta - 7.0(\sigma_p^+)_{G_\alpha}(\sigma_p^+)_{R_\alpha} - 5.8\sum(\sigma_p^+)_\alpha\sum(\sigma_m^+)_\beta + 1.64$. The carbenium ion character, common to both bromination and hydration, results in highly dissymmetric α- and β-substituent effects. However, these two reactions respond differently to β substituents: a β methyl increases the bromination rate but decreases the hydration rate. Similarities and differences in the transition-state models are discussed; the kinetic data suggest that the transition state is earlier in bromination than in hydration.

Quantitative treatment of the effects of π-donor substituents on reactivity has been extensively developed in aromatic series, but most of the treatments of substituents in aliphatic series include only alkyl groups or substituted alkyl groups where conjugation between the substituent and the reaction center is excluded.[2] The linear free-energy relationships (LFER) therefore contain only polar, steric, and hyperconjugative terms.[2b] Nevertheless, a few correlations including resonance parameters (albeit defined from reactions of aromatic compounds) have been proposed,[3-5] and recently Tidwell[6] put the hydration rates of a large set of aromatic and aliphatic ethylenes into a single correlation.

In this article, we develop a quantitative reactivity treatment based on new data on the bromination of enolic derivatives (enols, enol ethers, and enol esters) and phenylalkenes (unsubstituted phenyl ring). The assumption, made for hydration,[6] that the effects of substituents borne by the two unsaturated carbons are independent proves to be valid only to a first approximation. We shall show that a general equation including interactions between substituents[7] performs much better. These interaction terms will be related to the variation of the transition-state position with the nature of the conjugated electron-donating substituent; this variation is confirmed by measurements of the solvent effects upon the reactivity.

Scheme I

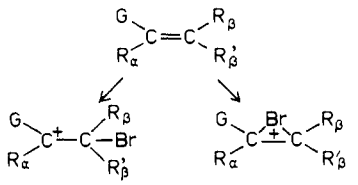

It is also possible to confirm by correlation analysis that the transition state is carbenium ion like for the compounds considered here. Contradictory statements have been made as to the carbenium (**1**, Scheme I) or bromonium (**2**) character of the transition state for Ad_EC1 bromine addition.[8] On the basis of a free-energy relationship (FER) using σ_I and σ_R parameters, Charton[5] concludes that the transition state is carbenium type; comparison of bromination with hydration and sulfenylation "reaction models" leads Schmid[9] to the opposite conclusion, that the transition state

(1) Ethylenic compounds reactivity: bromination, part 44. For part 43, see Blenvenüe-Goetz, E.; Dubois, J. E. *J. Chem. Res, Miniprint* **1979**, 2249-2269.
(2) (a) Exner, O. "Advances in LFER"; Chapman, N. B.; Shorter, J., Ed.; Plenum Press: London, 1972; p 1; (b) Taft, R. W. "Steric Effects in Organic Chemistry"; Newman, M. S., Ed.; Wiley: New York, 1956; Chapter 13.
(3) Charton, M.; Meislish, H. *J. Am. Chem. Soc.* **1958**, *80*, 5940-5943; Bowden, K. *Can. J. Chem.* **1965**, *43*, 3354-3363; de la Mare, P. B. D. *J. Chem. Soc.* **1960**, 3823-3826.
(4) Dubois, J. E.; Alcais, P.; Barbier, G.; Bienvenüe-Goetz, E. *Bull. Soc. Chim. Fr.* **1966**, 2113-2114.
(5) Charton, M.; Charton, B. I. *J. Org. Chem.* **1973**, *38*, 1631-1636, and previous articles in this series.
(6) (a) Oyama, K.; Tidwell, T. T. *J. Am. Chem. Soc.* **1976**, *98*, 947-951; (b) Koshy, K. M.; Roy, D.; Tidwell, T. T. *Ibid.* **1979**, *101*, 357-363.
(7) (a) Dubois, J. E.; Aaron, J. J.; Alcais, P.; Doucet, J. P.; Rothenberg, F.; Uzan, R. *J. Am. Chem. Soc.* **1972**, *94*, 6823-6828; (b) Argile, A., Doctoral Thesis, Université Paris VII, Paris, 1980.
(8) Garnier, F.; Dubois, J. E. *Bull. Soc. Chim. Fr.* **1968**, 3797-3803; in this mechanism, the rate-determining step is the unimolecular dissociation of the charge-transfer complex between olefin and bromine, leading to the positively charged intermediate.
(9) (a) Cerksus, T. R.; Czizmadia, V. M.; Schmid, G. H.; Tidwell, T. T. *Can. J. Chem.* **1978**, *56*, 205-210; (b) Schmid, G. H.; Tidwell, T. T. *J. Org. Chem.* **1978**, *43*, 460-463; this treatment is discussed in ref 34.

0002-7863/81/1503-5388$01.25/0